

Detect Everything with Few Examples

Xinyu Zhang, Yuting Wang, and Abdeslam Boularias

¹ Rutgers University

² {xz653,yw632,ab1544}@rutgers.edu

Abstract. Few-shot object detection aims at detecting novel categories given a few example images. Recent methods focus on finetuning strategies, with complicated procedures that prohibit a wider application. In this paper, we introduce DE-ViT, a few-shot object detector without the need for finetuning. DE-ViT’s novel architecture is based on a new region-propagation mechanism for localization. The propagated region masks are transformed into bounding boxes through a learnable spatial integral layer. Instead of training prototype classifiers, we propose to use prototypes to project ViT features into a subspace that is robust to overfitting on base classes. We evaluate DE-ViT on few-shot, and one-shot object detection benchmarks with Pascal VOC, COCO, and LVIS. DE-ViT establishes new state-of-the-art results on all benchmarks. Notably, for COCO, DE-ViT surpasses the few-shot SoTA by 15 mAP on 10-shot and 7.2 mAP on 30-shot and one-shot SoTA by 2.8 AP50. For LVIS, DE-ViT outperforms few-shot SoTA by 20 box AP_r.

1 Introduction

Object recognition and localization are two of the core tasks in computer vision. *Few-shot object detection* provides a promising paradigm for generic object detectors by representing novel categories with a set of support images [2]. However, despite the promising practicality in principle, most recent few-shot methods rely on finetuning to adapt to novel classes [28], which is often a complicated and tedious procedure that limits the practical use of these methods and that results in a large accuracy gap between base and novel classes [55].

Motivated by the recent progress in unsupervised object discovery with pre-trained vision transformers (ViTs) [36, 43], strong pretrained ViTs can also be used to overcome the limitations of finetuning. However, despite their rich semantic representations, pretrained ViT features lack the coordinates information that is required to perform a bounding box regression. As shown in Sec. 4.2, naively applying a conventional regression on ViT features yields poor localization results, while unfreezing the ViT backbone leads to an accuracy collapse on novel classes, by completely overfitting the base classes.

Preprint.

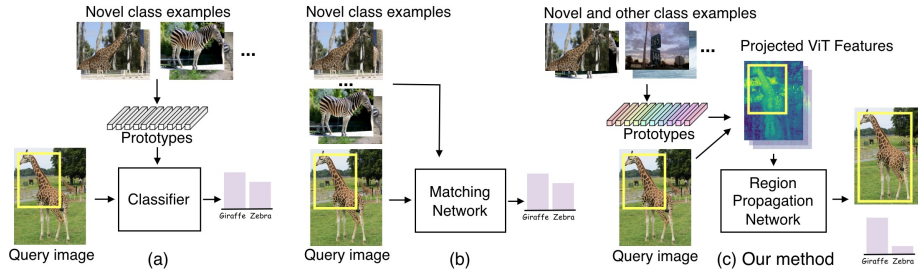


Fig. 2: Existing meta-learning-based FSOD methods can be divided into two categories (a and b). Methods in the first category (a) build prototypes from novel class examples and use these prototypes as the classifier weights of a detection network. Despite its simplicity, this strategy exhibits inferior accuracy [28]. Methods in the second category (b) learn to match the proposal regions in the query image and novel examples through a matching network. This strategy is computationally heavy due to dense feature interactions across multiple images and usually requires finetuning to increase accuracy in novel classes [18, 19]. In contrast, our method (c) applies a dot-product with the prototypes to project ViT features into a subspace that is robust to overfitting on base classes, and then applies a region propagation network to refine the localization and derive the class score. Our method does not employ any finetuning for novel classes.

2 Related work

Few-shot Object Detection (FSOD) aims at detecting objects of novel classes by utilizing a few support images from novel classes as training samples [28]. Existing approaches can be broadly classified into finetuning-based [11, 14, 45, 46, 50] and meta-learning-based strategies [10, 25, 51]. Finetuning-based methods, despite their prevalence, suffer from a large accuracy gap between the base and novel classes, as well as practical limitations due to redundant multi-stage procedures [55]. Meta-learning-based methods avoid finetuning through online adaptation. Early works on meta-learning FSOD (Fig. 2.a) construct prototypes from novel class examples and use the prototypes as input to a network that classifies query images [25, 51]. Recent methods (Fig. 2.b) design interaction mechanisms of dense spatial features between query and support images [17–19]. In contrast, our method (Fig. 2.c) computes dot-products with the prototypes to project their features into a subspace, instead of using a prototype classifier, and applies a region-propagation network instead of a dense feature matching network. One-shot Object Detection (OSOD) is an extreme case of FSOD with only one example per novel class, it reduces the setting to single-class detection [52].

Vision Transformer (ViT) is a recent network architecture that demonstrates stronger performance and more interpretable features than traditional convolutional architectures. There is a growing trend of applying self-supervised ViTs, such as DINO [5, 39], to unsupervised object discovery [41, 43, 54, 59]. Token-Cut [47] applies graph-cut over DINO features to separate the primary foreground object. DeepSpectral [36] predicts semantic segmentation masks without supervision through spectral clustering over DINO features. OW-DETR [16] uses

DINO ViT to discover unknown objects in an open-world setting. In this work, we use pretrained ViTs for solving the few-shot object detection problem.

3 Method

3.1 Problem Formulation

We use \mathcal{C} to denote the set of classes. In few-shot object detection (FSOD), \mathcal{C} is composed of a set of base classes, denoted by \mathcal{C}_{base} , and a set of novel classes, denoted by \mathcal{C}_{novel} . Thus, $\mathcal{C} = \mathcal{C}_{base} \cup \mathcal{C}_{novel}$ and $\mathcal{C}_{base} \cap \mathcal{C}_{novel} = \emptyset$. During training, a large number of examples are provided for the base classes. During testing, only k labeled samples are provided for each novel class. The samples for novel classes are referred to as *support images*. The goal of FSOD is to leverage the training data of \mathcal{C}_{base} to learn a detector that can detect objects of \mathcal{C}_{novel} given the k -shot support images.

3.2 Region Propagation Network

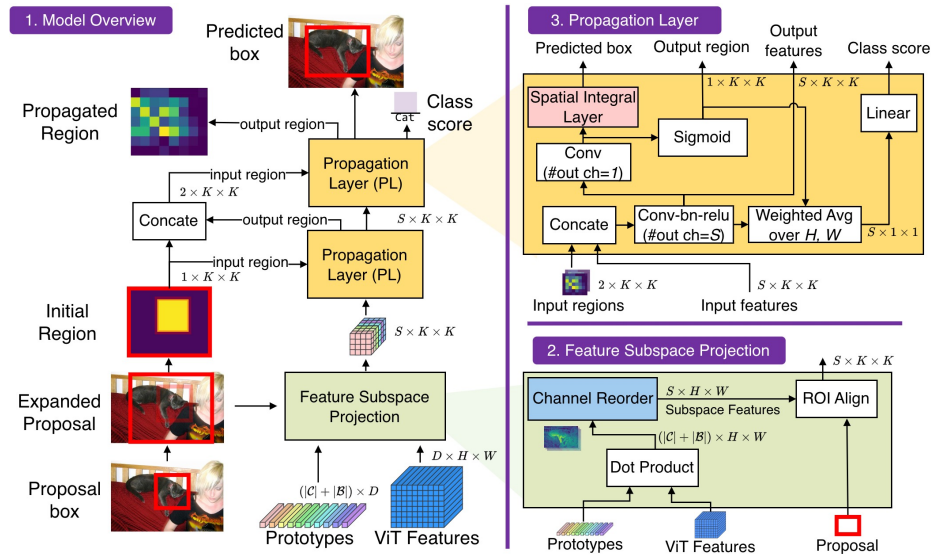


Fig. 3: Overall framework of our proposed method. Given a proposal box of a query image, we extract the initial mask region (shown here in yellow) and expand the proposal by a constant ratio. Next, the region within the expanded proposal is gradually propagated and refined to fit the object area through a sequence of propagation layers. Each propagation layer accepts previous regions and features as input while returning updated features and region as outputs. The final predicted region is transformed to bounding box coordinates through a learnable spatial integral layer, as detailed in Sec. 3.3. The predicted region also serves as spatial attention and is used for a weighted averaging of the features along height and width. The averaged features are then mapped to class scores. The projected features are the dot products between the ViT features of a given query image and class prototypes, as detailed in Sec. 3.4.

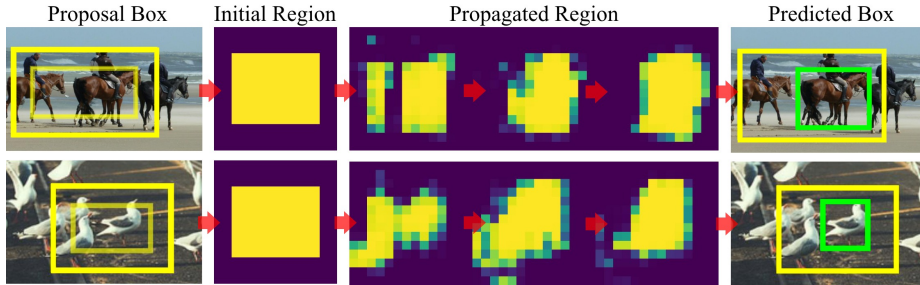


Fig. 4: Visualizations of region propagation on classes “horse” and “birds” (first and second row). The proposal, expanded proposals, and final predicted boxes are colored in transparent yellow, yellow, and green, respectively. The three propagated regions (from left to right) are sampled from the output of the first three PL blocks in ascending order.

Despite having rich semantics information, pretrained ViT features lack the coordinates information required for bounding box regression. As shown in Sec. 4.2, naively applying a conventional regression on ViT features yields poor localization results. A natural solution is to learn this localization capability by finetuning the ViT backbone during the training of the detector with the base classes. However, we observed that finetuning results in completely overfitting the base classes and in an accuracy collapse on novel classes. This was observed when integrating DINOv2 ViT into the framework of Meta RCNN [51], a standard prototype-based FSOD, as shown in Sec. 4.2. This suggests that harnessing the generalization power of strong ViT backbones for FSOD is non-trivial. The question here is how to produce accurate localization with pretrained ViT features.

Given an object proposal, we use a region propagation network that gradually propagates the proposal region to accurately cover and fit the object by refining an object mask. Unlike bounding box regression, mask prediction localizes objects without coordinate outputs. The propagated region is then transformed into a bounding box through a learnable spatial integral layer. We use an off-the-shelf region proposal network (RPN) to generate the initial region proposals, as class-agnostic proposals are shown to generalize well to novel classes [13]. Each proposal is expanded by a fixed ratio in order to delimit the propagation boundaries. The overall framework is shown in Fig. 3.

Propagation Layer. We propose the region *Propagation Layer* (PL), a new type of network module designed for object detection. PL serves as the central building block of our method. An example is shown in Fig. 4. The t -th PL block takes all previous regions $r_{0:t-1} \in \mathbb{R}^{t \times K \times K}$ and the previous PL block features $h_{t-1} \in \mathbb{R}^{S \times K \times K}$ as input, where t denotes the number of PL blocks, S denotes the number of feature channels, and K denotes the feature spatial size. The t -th PL block outputs the updated region $r_t \in \mathbb{R}^{1 \times K \times K}$, features $h_t \in \mathbb{R}^{S \times K \times K}$, bounding box $b_t \in \mathbb{R}^4$, and class score $c_t \in \mathbb{R}$. Each PL block works as a small detection network and can be stacked to improve accuracy. The update rule is explained in Eq. 1 and illustrated in the third part of Fig. 3.

$$\begin{aligned}
h_t &= f_{\text{update},t}(\text{concat}(r_{0:t-1}, h_{t-1}); \theta), \quad h_{t,\text{region}} = f_{\text{region},t}(h_t; \theta) \\
r_t &= \sigma(h_{t,\text{region}}), \quad b_t = f_{\text{integral},t}(h_t, r_t; \theta) \\
c_t &= f_{\text{class},t}(\text{WeightedAvgPool}(h_t, r_t); \theta)
\end{aligned} \tag{1}$$

In Eq. 1, $f_{\text{update},t}$ denotes the conv-bn-relu block with S output channels that updates the hidden features, and concat denotes channel-wise concatenation. $f_{\text{region},t}$ denotes the conv block with single channel output that predicts the output region logits $h_{t,\text{region}} \in \mathbb{R}^{1 \times K \times K}$. σ denotes the sigmoid function. $f_{\text{integral},t}$ denotes the spatial integral layer detailed in Sec. 3.3. h_t is aggregated over spatial dimensions to $\text{WeightedAvgPool}(h_t, r_t) \in \mathbb{R}^{S \times 1 \times 1}$ with weights r_t . $f_{\text{class},t}$ denotes the linear block that maps $\text{WeightedAvgPool}(h_t, r_t)$ to class scores. θ denotes network parameters. During training, we use focal loss and L1 regression loss for the output class score c_t and bounding box b_t . For the output region r_t , we apply BCE loss and Dice loss [44]. The region labels during training are generated by the ground-truth object region within the expanded proposals.

3.3 Learnable Spatial Integral

Converting masks to bounding boxes is a widely-used transformation in instance segmentation networks [40] as a post-processing step. The standard solution is to find the top-left and bottom-right foreground pixels and use their positions as the bounding box coordinates [35]. However, this approach has major limitations. Firstly, this mask-to-box conversion assumes the availability of ground-truth instance masks, which are much more expensive to obtain than bounding boxes [31]. Moreover, this approach is non-differentiable and is also prone to outliers. Therefore, the question is how to accurately derive bounding boxes from the region-based localization results using a learnable and differentiable function.

Let $b^{\text{out}} = (c_w^{\text{out}}, c_h^{\text{out}}, w^{\text{out}}, h^{\text{out}})$ denote the output bounding box, where $c_w^{\text{out}} \in [0, W]$, $w^{\text{out}} \in [0, W]$ and $c_h^{\text{out}} \in [0, H]$, $h^{\text{out}} \in [0, H]$. Instead of predicting b^{out} directly, we propose to first predict a relative bounding box $b^{\text{rel}} = (c_w^{\text{rel}}, c_h^{\text{rel}}, w^{\text{rel}}, h^{\text{rel}}) \in [0, 1]^4$, that can be transformed to b^{out} according to Eq. 2,

$$\begin{aligned}
(w^{\text{out}}, h^{\text{out}}) &= (w^{\text{exp}} w^{\text{rel}}, h^{\text{exp}} h^{\text{rel}}), \\
(c_w^{\text{out}}, c_h^{\text{out}}) &= (c_w^{\text{exp}} - 0.5w^{\text{exp}}, c_h^{\text{exp}} - 0.5h^{\text{exp}}) + (c_w^{\text{rel}} w^{\text{exp}}, c_h^{\text{rel}} h^{\text{exp}}),
\end{aligned} \tag{2}$$

where $b^{\text{exp}} = (c_w^{\text{exp}}, c_h^{\text{exp}}, w^{\text{exp}}, h^{\text{exp}})$ denotes the expanded proposal. Thus, b^{rel} is a normalized bounding box relative to b^{exp} . Let $h_{\text{region}} \in \mathbb{R}^{K \times K}$ denote the output region logits, where we skip the notation of t -th block and the channel of 1 for simplicity. Our spatial integral layer f_{integral} estimates b^{rel} with Eq. 3 and 4. An illustrative example is given in Fig. 5.

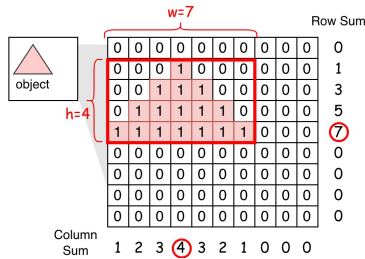


Fig. 5: The max row sum and column sum are used as the box width and height of the triangular object.

To motivate Eq. 3 and 4, consider the toy example of converting a binary triangle mask to a bounding box in Fig. 5. A reasonable approach is to compute the mask center as the bounding box center and use the max row sum and column sum as width and height. Inspired by this insight, we compute the expected position of the spatial distribution $\text{softmax}(h_{region})$ as the center of b^{rel} in Eq. 3. We compute the row and column sums of the output region as $\sum_{j=1}^K \sigma(h_{region})_{ij}$ and $\sum_{i=1}^K \sigma(h_{region})_{ij}$ in Eq. 4. Instead of picking the maximum, we apply a soft aggregation to average all row or column sums in terms of magnitude rank. The aggregation is done by sorting the row and column sums, and then computing the weighted average. This explains the use of order statistics notation (i) and (j) . Parameters $\theta^{\mathbf{h}} \in \mathbb{R}^K$, $\theta^{\mathbf{w}} \in \mathbb{R}^K$ are learnable aggregation weights.

3.4 Feature Subspace Projection

A major challenge of FSOD is to generalize to novel classes that are unseen during training. However, despite numerous attempts to solving this problem, by using margin-based regularization for example [34], there persists a considerable accuracy gap between base and novel classes [2]. This disparity indicates that a network trained with base classes would inevitably overfit on patterns that are only present among the base classes. A classic technique to reduce overfitting consists in representing data in a low-rank subspace [42]. We explore in this work the construction of a subspace of pre-trained ViT features that reduces the accuracy gap between base and novel classes.

Prototypes are class representatives built from support images. Given the support images of each class, we compute the ViT features, crop the features with object bounding boxes and use the average feature as the class prototype [51]. Let $p_{\mathcal{C}} \in \mathbb{R}^{|\mathcal{C}| \times D}$ denote the prototypes of classes from set \mathcal{C} , where D denotes the channel dimension. Let $h_{vit} \in \mathbb{R}^{D \times H \times W}$ denote the ViT features of the query image. We assume that both prototypes and features are normalized to unit length at the channel dimension. Then $p_{\mathcal{C}} \cdot h_{vit} \in \mathbb{R}^{|\mathcal{C}| \times H \times W}$ can be interpreted as a subspace projection with $p_{\mathcal{C}}$ being the basis. However, this subspace construction has two limitations. Firstly, only using prototypes of classes set \mathcal{C} can be too limited to sufficiently capture the feature information.

$$(c_w^{\text{rel}}, c_h^{\text{rel}}) = \sum_{i,j=1}^{K,K} \left(\frac{i}{K}, \frac{j}{K} \right) * \text{softmax}(h_{region})_{ij} \quad (3)$$

$$w^{\text{rel}} = \sum_{i=1}^K \sum_{j=1}^K \frac{\sigma(h_{region})_{(i)j}}{K} \theta^{\mathbf{w}}_i \quad (4)$$

$$h^{\text{rel}} = \sum_{j=1}^K \sum_{i=1}^K \frac{\sigma(h_{region})_{i(j)}}{K} \theta^{\mathbf{h}}_j$$

Table 1: Results on COCO 2014 few-shot benchmark. Our method outperforms existing work in detecting novel classes by a significant margin. Results surpassing the SoTA are indicated in bold.

Method	Finetune	10-shot				30-shot				
		on Novel	bAP	nAP	nAP50	nAP75	bAP	nAP	nAP50	nAP75
FSRW [25]	✗	-	5.6	12.3	4.6	-	9.1	19	7.6	
Meta R-CNN [51]	✗	5.2	6.1	19.1	6.6	7.1	9.9	25.3	10.8	
TFA [46]	✓	33.9	10	19.2	9.2	34.5	13.5	24.9	13.2	
Multi-Relation Det [10]	✗	-	16.6	31.3	16.1	-	-	-	-	
FSCE [45]	✓	-	11.9	-	10.5	-	16.4	-	16.2	
Retentive RCNN [11]	✓	39.2	10.5	19.5	9.3	39.3	13.8	22.9	13.8	
HeteroGraph [17]	✓	-	11.6	23.9	9.8	-	16.5	31.9	15.5	
FsDetView [50]	✓	6.4	7.6	-	-	9.3	12	-	-	
Meta Faster RCNN [18]	✓	-	12.7	25.7	10.8	-	16.6	31.8	15.8	
LVC [26]	✓	28.7	19	34.1	19	34.8	26.8	45.8	27.5	
CrossTransformer [19]	✓	-	17.1	30.2	17	-	21.4	35.5	22.1	
NIFF [14]	✓	39	18.8	-	-	39	20.9	-	-	
DiGeo [34]	✓	39.2	10.3	18.7	9.9	39.4	14.2	26.2	14.8	
DE-ViT	ViT-S/14	✗	24	27.1	43.1	28.4	24.2	26.9	43.1	28.5
(Ours)	ViT-B/14	✗	28.3	33.2	51.4	35.5	28.5	33.4	51.4	35.7
	ViT-L/14	✗	29.4	34.0	52.9	37.0	29.5	34.0	53.0	37.2

Secondly, a permutation of \mathcal{C} creates a different but equivalent subspace, yet designing permutation-invariant networks is a highly challenging problem [22]. For the first limitation, we introduce a set \mathcal{B} of background classes, $\mathcal{B} \cap \mathcal{C} = \emptyset$, with $p_{\mathcal{B}} \in \mathbb{R}^{|\mathcal{B}| \times D}$ being the prototypes of \mathcal{B} , to preserve more information from h_{vit} . For the second limitation, we propose to build a separate subspace for each class $c \in \mathcal{C}$, and reorder other classes $\mathcal{C} \setminus c$ to resolve permutation ambiguity. The feature subspace projection is explained in Eq. 5 and illustrated in Fig. 3.

$$h_{subspace,c} = \text{concat}(p_c \cdot h_{vit}, \text{channel-reorder}(p_{\mathcal{C} \setminus c} \cdot h_{vit}), p_{\mathcal{B}} \cdot h_{vit}) \quad (5)$$

In Eq. 5, $h_{subspace,c} \in \mathbb{R}^{S \times H \times W}$ denotes the subspace feature for class c , and function channel-reorder sorts channels by magnitude and then interpolates $|\mathcal{C}| - 1$ channels to a pre-defined number of channels. In practice, we use example images of non-object stuff classes, *e.g.*, sky, road, floor, to construct \mathcal{B} . As shown in Sec. 4.2, feature subspace projection significantly reduces the accuracy gap between base and novel classes. On the other hand, creating a subspace for each class $c \in \mathcal{C}$ introduces costly per-class inference. However, the per-class inference cost can be reduced by finding the top T most likely classes with a lightweight prototype classifier [51] and only performing inference for these T classes. As shown in Sec. 4.2, our method achieves a faster inference speed and surpasses SoTA when $T = 3$.

4 Experiments

We comprehensively evaluate our method on few-shot and one-shot benchmarks. Furthermore, we compare the efficiency of our method against SoTA solutions,

Table 2: nAP50 results on Pascal VOC few-shot benchmark. Results surpassing the SoTA are indicated in bold. (*) denotes that implementation is not publicly available.

Method	Novel Split 1					Novel Split 2					Novel Split 3					Avg
	1	2	3	5	10	1	2	3	5	10	1	2	3	5	10	
TFA [46]	39.8	36.1	44.7	55.7	56.0	23.5	26.9	34.1	35.1	39.1	30.8	34.8	42.8	49.5	49.8	39.9
FsDetView	25.4	20.4	37.4	36.1	42.3	22.9	21.7	22.6	25.6	29.2	32.4	19	29.8	33.2	39.8	29.2
Multi-Relation Det [10]	37.8	43.6	51.6	56.5	58.6	22.5	30.6	40.7	43.1	47.6	31	37.9	43.7	51.3	49.8	43.1
Retentive RCNN [11]	42.4	45.8	45.9	53.7	56.1	21.7	27.8	35.2	37.0	40.3	30.2	37.6	43	49.7	50.1	41.1
Meta Faster R-CNN [18]	43.0	54.5	60.6	66.1	65.4	27.7	35.5	46.1	47.8	51.4	40.6	46.4	53.4	59.9	58.6	50.5
LVC [26]	54.5	53.2	58.8	63.2	65.7	32.8	29.2	50.7	49.8	50.6	48.4	52.7	55	59.6	59.6	52.3
CrossTransformer [19]	49.9	57.1	57.9	63.2	67.1	27.6	34.5	43.7	49.2	51.2	39.5	54.7	52.3	57	58.7	50.9
HeteroGraph [17]	42.4	51.9	55.7	62.6	63.4	25.9	37.8	46.6	48.9	51.1	35.2	42.9	47.8	54.8	53.5	48.0
DiGeo [34]	37.9	39.4	48.5	58.6	61.5	26.6	28.9	41.9	42.1	49.1	30.4	40.1	46.9	52.7	54.7	44.0
NIFF [14] (*)	62.8	67.2	68.0	70.3	68.8	38.4	42.9	54.0	56.4	54	56.4	62.1	61.2	64.1	63.9	59.4
DE-ViT	47.5	64.5	57.0	68.5	67.3	43.1	34.1	49.7	56.7	60.8	52.5	62.1	60.7	61.4	64.5	57.7
(Ours)	56.9	61.8	68.0	73.9	72.8	45.3	47.3	58.2	59.8	60.6	58.6	62.3	62.7	64.6	67.8	61.4
	55.4	56.1	68.1	70.9	71.9	43.0	39.3	58.1	61.6	63.1	58.2	64	61.3	64.2	67.3	60.2

study few-shot performance for different numbers of shots, compare it to language-based detectors, and provide qualitative results. We conduct ablations to study the contributions of the proposed components to the performance of our method. Our source code and the pretrained models will be publicly released upon acceptance.

Evaluation Metrics and Datasets. Few-shot and one-shot evaluations split classes into base and novel classes. Base classes are seen during training and novel classes are unseen. The performance on novel classes is more important. For COCO and Pascal VOC, nAP, nAP50, and nAP75 represent mAP, AP50, and AP75 in novel classes. bAP and bAP50 represent mAP and AP50 in base classes. One-shot evaluation conventionally divides 80 classes of COCO into four even partitions, and alternatively uses three as base classes and one partition as novel classes [37]. There are 4 base/novel splits in total, named Split-1/2/3/4. For LVIS, APr, APc, and APf represent AP on rare, common, and frequent categories. Rare categories are used as novel classes. Metrics on LVIS, such as box APr and mask APr, are computed on bounding boxes and on instance segmentation masks separately. We evaluate our method on Pascal VOC [9], COCO [31], and LVIS-v1 [15]. We follow the conventional base/novel classes split and use the same support images of novel classes with existing work [46, 52].

Implementation Details. We adopt a standard two-stage object detection framework, similarly to Mask R-CNN [20]. We use the same off-the-shelf RPN with existing work [56] to generate object proposals. The RPN is trained separately for each dataset using only base classes. We use DINOv2 [39] ViT as the backbone unless specified, and report results in ViT-S/B/L (small, base, large) model sizes. The ViT backbones are kept frozen during detector training. We adopt the prototype extraction procedure of Meta RCNN [51] using ViT features. Prototypes of background classes set \mathcal{B} are extracted from images of stuff (non-object) classes, *e.g.*, sky, road, from COCOStuff [3] unless specified. Similar to [51], the top T most likely classes for each proposal are determined by the distances between prototypes and the average proposal feature. We set

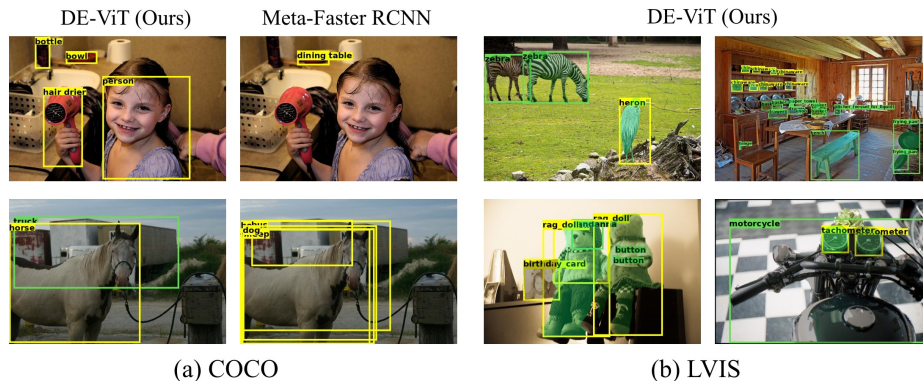


Fig. 6: Qualitative visualization of our method DE-ViT on COCO (a) and LVIS (b), and comparison to Meta-Faster RCNN [18]. Boxes of base and novel classes are colored in green and yellow, respectively.

T to 10 unless specified, where T is the number of classes to create subspace features and perform inference as explained in Sec. 3.4. We apply 3 PL blocks for experiments on Pascal VOC and COCO, and 5 PL blocks for those on LVIS.

4.1 Main Results

Tab. 1 shows our results on the few-shot COCO benchmark. Our method DE-ViT outperforms the previous SoTA LVC [26] by a significant margin (+15 nAP on 10-shot, +7.2 nAP on 30-shot). It is worth noting that LVC requires over ten stages for self-training and pseudo-labeling procedures on novel classes [1], while our method DE-ViT is trained once on the base classes and used directly on the novel classes. A pretrained model for LVC has never been released. We plot the nAP50 of our method and the SoTAs with different numbers of shots in Fig. 7.

Table 3: Performance comparison with existing FSOD methods on the LVIS dataset. We report the box AP.

Method	APr	APc	APf	AP	
DiGeo [34]	16.6	22.8	28	24.4	
DE-ViT (Ours)	ViT-S/14	23.4	22.8	22.5	22.8
	ViT-B/14	26.8	26.5	25.3	26
	ViT-L/14	33.6	30.1	30.7	30.9

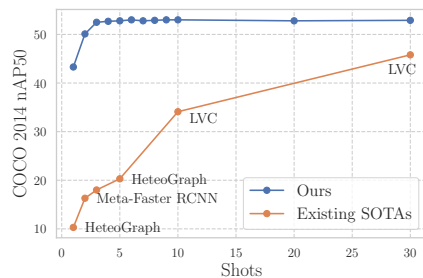


Fig. 7: Performance of DE-ViT and few-shot SoTA with different numbers of shots.

Table 4: Results on COCO 2017 one-shot benchmark. DE-ViT outperforms existing work and is not limited to single class detection and single support image as other one-shot methods.

	bAP50					nAP50				
	Split-1	Split-2	Split-3	Split-4	Avg	Split-1	Split-2	Split-3	Split-4	Avg
SiamMask [37]	38.9	37.1	37.8	36.6	37.6	15.3	17.6	17.4	17	16.8
CoAE [23]	42.2	40.2	39.9	41.3	40.9	23.4	23.6	20.5	20.4	22
AIT [6]	50.1	47.2	45.8	46.9	47.5	26	26.4	22.3	22.6	24.3
SaFT [55]	49.2	47.2	47.9	49	48.3	27.8	27.6	21	23	24.9
BHRL [52]	56	52.1	52.6	53.4	53.6	26.1	29	22.7	24.5	25.6
DE-ViT (Ours, ViT-L/14)	59.4	57.0	61.3	60.7	59.6	27.4	33.2	27.1	26.1	28.4

Tab. 2 shows our results on the few-shot Pascal VOC benchmark. Our method DE-ViT outperforms the previous SoTA NIFF [14] by +2.0 on averaged nAP50. It is worth noting that the implementation of NIFF has not been released.

LVIS has been regarded as a highly challenging benchmark for FSOD [46] with 337 novel classes and only DiGeo [34] reports few-shot results on LVIS v1. Tab. 3 shows that our method outperforms DiGeo in all metrics and a significant boost in the accuracy of detecting novel objects (+20 box APr).

Tab. 4 shows our results on the one-shot COCO benchmark. DE-ViT surpasses the previous SoTA BHRL by 6 bAP50 and 2.8 nAP50. One-shot object detection task follows a single-class detection setting. Therefore, we adapt our method DE-ViT by detecting each class separately during evaluation. OWL-ViT [38] also reports one-shot results on COCO. However, OWL-ViT’s results are obtained with an ensemble of language-based detection and one-shot pipelines without providing an implementation or isolated measurements. Therefore, we exclude OWL-ViT from the one-shot comparison.

4.2 Analysis and Ablation Studies

Efficiency. We compare the inference time of DE-ViT with different values of T against recent few-shot works in Tab. 5 in COCO 10-shots setting, where Swin denotes Swin Transformer [32], RN101 denotes ResNet101 [21], MFRCNN denotes Meta Faster RCNN [18], and CrossT denotes Cross Transformer [19]. T is the number of classes to create subspace features and perform inference. Tab. 5 shows that our method DE-ViT can achieve the smallest inference time while having better accuracy. The inference times of all the compared methods are measured on the same machine.

Qualitative results. Fig. 4 shows examples of region propagations on classes “horse” and “bird”. The regions gradually move from the initial proposal region toward the object regions and are transformed into predicted boxes with our spatial integral layer. Fig. 6 shows a qualitative demonstration of our method on COCO and LVIS, and a comparison to Meta Faster RCNN [18]. Note that we chose Meta Faster RCNN over other existing works because of the availability

Table 5: Ablation study on different values of T and inference time comparison with existing methods. N/A: The pretrained model is not publicly available for evaluation.

Method	Backbone	T	nAP50	Secs/Img
DE-ViT (Ours)	ViT-L/14	1	49.6	0.22
		3	52.5	0.33
		10	52.9	0.83
LVC [26]	Swin-S	-	34.1	N/A
MFRCNN [18]	RN101	-	25.7	0.61
CrossT [19]	Custom	-	30.2	3

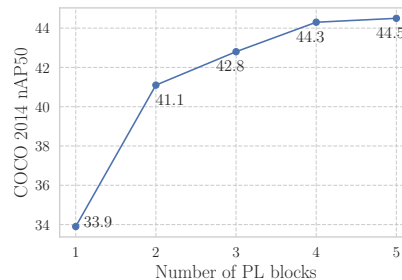


Fig. 8: Ablation study of our method on different numbers of PL blocks with ViT-S/14 backbone.

of its pretrained models. DE-ViT detects more novel objects while having fewer false positives. We provide more visualizations in the supplementary material.

Table 6: Comparison to language-based detectors on LVIS and COCO 2017. †: use customized pretrained backbone instead of public ones. “-”: result that was not reported.

Method	Backbone	Use Extra Training Set	LVIS		COCO
			mask AP _r	box AP _r	nAP50
ViLD [13]	EffNet-B7	✗	26.3	27	27.6
RegionCLIP [56]	RN50x4	✓	-	22	39.3
OV-DETR [53]	ViT-B/32	✗	-	17.4	29.4
Detic [58]	RN50	✓	17.8	-	27.8
OWL-ViT [38]	ViT-L/14 [†]	✗	-	25.6	-
OWL-ViT [38]	ViT-L/14 [†]	✓	-	31.2	-
CORA ⁺ [49]	RN50x4	✓	-	28.1	43.1
Ro-ViT [27]	ViT-L/14 [†]	✗	31.4	-	33
Co-Det [33]	Swin-B	✓	29.4	-	30.6
F-VLM [27]	RN50x64	✗	32.8	-	28.0
DE-ViT (Ours, 30-shots)	ViT-S/14	✗	24.2	23.4	39.5
	ViT-B/14	✗	28.5	26.8	45.4
	ViT-L/14	✗	34.3	33.6	50

Comparison to language-based detectors. Tab. 6 compares our method DE-ViT against language-based detectors on the COCO and LVIS-v1 datasets. Language-based detection, also known as open-vocabulary detection [48], does not assume access to support images on novel classes but requires the knowledge of the novel class names. The class names are then used to discover images of novel classes from a large collection of image-text pairs. Therefore, language-based detectors have the following limitations. First, many objects lack clear

Table 7: Ablation studies on the feature subspace projection.

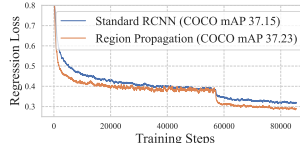
Raw Feature Input Prototype Classifier	Feature Subspace Projection			Novel		Base	
	c	\mathcal{B}	$\mathcal{C} \setminus c$	nAP50	nAP75	bAP50	bAP75
✓				4.5	2.2	48.9	22.5
	✓			26.2	9.7	29.3	12
	✓	✓		38.4	23	43.4	26.8
	✓	✓	✓	39.5	24.1	42.3	25.9

Table 9: Ablation studies on the region propagation-based localization.

Conventional Regression Net	Expanded Proposal	Region Propagation Network	Novel		Base	
			nAP50	nAP75	bAP50	bAP75
✓			37.7	14.6	46.5	23.9
	✓		35.6	12.5	41.3	19.8
		✓	39.5	24.1	42.3	25.9

Table 8: Ablation studies on the background classes set \mathcal{B} .

Background Classes \mathcal{B}	nAP50	bAP50
COCostuff [3]	43.1	45.6
ADE20k [57]	42.5	45.8
ADE20k (all)	42.1	44.7

**Fig. 9:** Regression loss curves and mAP of using standard RCNN and region propagation in supervised object detection.

names [30], *e.g.*, objects that are specific to certain contexts [24]. Second, the association between visual concepts and language is evolving and not static [8]. In contrast, few-shot object detection (FSOD) does not assume any knowledge of class names, and novel classes are described with support images only. FSOD’s setting is therefore more general and arguably more challenging, and aims to emulate humans’ capability to recognize objects by their consistent appearance.

In COCO, our method DE-ViT outperforms the previous SoTA CORA⁺ by 6.9 AP50. Our method only trains on COCO while CORA⁺ uses ImageNet-21K [29] and COCO Captions [7] as additional training data. In LVIS, DE-ViT outperforms the previous SoTA on mask APr (+1.5 over F-VLM) and box APr (+2.4 over OWL-ViT). Note that we report the Co-Det [33] result with Swin-B backbone instead of EVA02-L backbone [12] because the latter includes the base and novel classes of COCO in its training set. Moreover, we observe a high variance in the performance of language-based detectors. F-VLM achieves a mask APr of 32.8 on LVIS but only has 28 nAP50 on COCO. While CORA⁺ has 43.1 nAP50 on COCO but only a box APr of 28.1 on LVIS. On the contrary, our method DE-ViT outperforms existing solutions on both LVIS and COCO.

Feature subspace projection. We examine the component effects for feature subspace projection in Tab. 7. The first column represents the integration of raw features of DINOv2 ViT into Meta RCNN [51], a standard prototype-based few-shot detector. Tab. 7 shows that the model has an accuracy collapse on novel classes with raw ViT feature inputs by completely overfitting base classes. The c , \mathcal{B} , and $\mathcal{C} \setminus c$ represents different groups of prototypes used in feature projection, as in Eq. 5. By projecting features to p_c , general detection ability emerges (nAP50: 4.5 \rightarrow 26.2), then significantly improves after adding background classes prototypes $p_{\mathcal{B}}$ (nAP50: 26.2 \rightarrow 38.4), and further improves with $p_{\mathcal{C} \setminus c}$ (nAP50: 38.4 \rightarrow 39.5). Results in Tab. 7 and 9 are obtained on COCO 2017 with ViT-S/14.

Region propagation network. We study the impacts of region-propagation-based localization in Tab. 9. The conventional regression network exhibits poor localization accuracy on novel classes (nAP75: 14.6), and simply expanding proposals even lowers the performance (nAP75: 14.6 \rightarrow 12.5). When using our proposed region-propagation network with the learnable spatial integral layer, the localization accuracy has a significant boost (nAP75: 12.5 \rightarrow 24.1). Note that the results in Tab. 9 are obtained by only changing the localization architectures while keeping the feature subspace projection.

Number of propagation layers. We study the impacts of the number of PL blocks in Fig. 8, which shows that stacking more PL blocks consistently improves accuracy. The accuracy saturates around 5 blocks and there is still non-negligible improvement from 3 \rightarrow 4 blocks. Note that we use 3 blocks in our COCO and Pascal VOC experiments and 5 blocks in LVIS ones.

Background classes set \mathcal{B} . We study the impacts of using different background classes sets \mathcal{B} in Tab. 8. The first and second rows represent using the stuff (non-object) classes, *e.g.*, floor, sky, of COCOstuff [3] and ADE20k [57] to construct \mathcal{B} . Note that COCOstuff has 53 stuff classes and ADE20k has 35 stuff classes, which explains the minor accuracy drop from ADE20k. The third row denotes using all classes of ADE20k as \mathcal{B} . This indicates that adding thing (object) classes to \mathcal{B} may not be beneficial. Tab. 8 shows that changing \mathcal{B} only results in small accuracy variations. This suggests that our proposed feature subspace projection does not rely on specific prototypes.

Supervised object detection through region propagation. We further study the application of our proposed techniques in supervised object detection. In Fig. 9, we compare the mAPs and regression loss curves of a standard RCNN head and using region propagation for RCNN prediction in COCO detection. We use a ResNet-50 backbone and the same number of parameters for each head. Despite having similar mAPs (37.15 vs. 37.23), Fig. 9 shows that our proposed region propagation produces a consistently lower regression loss than the standard RCNN. This suggests the potential of our proposed techniques in object detection tasks.

We provide further analysis on the effects of the number of shots, scenarios when expanded proposals cover multiple same-class objects, and more qualitative visualizations in the supplementary document.

5 Discussion and Conclusion

In this work, we have proposed a region-propagation-based localization architecture, a learnable spatial integral layer to transform masks to bounding boxes, and a feature subspace projection to reduce the accuracy gap between base and novel classes. With these three novel techniques, our method DE-ViT establishes a new state-of-the-art on the few-shot object detection benchmarks.

Some open questions are still, however, worth discussing. Our region propagation network and spatial integral layer are not limited to few-shot object de-

tection, and can be straightforwardly extended to support segmentation output. This suggests the potential for generalizing these techniques to become standard building blocks for object detection, and solving detection tasks through segmentation, but this possibility is not fully explored in this work. One limitation of our approach is that our feature subspace projection creates separate features for each class, which introduces inference overhead. It is possible to design a class-level attention mechanism to remove this overhead. Finally, we hope that our work will be useful in downstream tasks such as robotic manipulation, and help other researchers develop better methods for few-shot object detection.

References

1. Official repo: "label, verify, correct: A simple few-shot object detection method". <https://github.com/prannaykaul/lvc>, (Accessed on 11/17/2023) **10**
2. Antonelli, S., Avola, D., Cinque, L., Crisostomi, D., Foresti, G.L., Galasso, F., Marini, M.R., Mecca, A., Pannone, D.: Few-shot object detection: A survey. *ACM Computing Surveys (CSUR)* **54**(11s), 1–37 (2022) **1, 7**
3. Caesar, H., Uijlings, J., Ferrari, V.: Coco-stuff: Thing and stuff classes in context. In: *Proceedings of the IEEE Conference on Computer Vision and Pattern Recognition*. pp. 1209–1218 (2018) **9, 13, 14**
4. Calli, B., Singh, A., Walsman, A., Srinivasa, S., Abbeel, P., Dollar, A.M.: The ycb object and model set: Towards common benchmarks for manipulation research. In: *International Conference on Advanced Robotics (ICAR)*. pp. 510–517. *IEEE* (2015) **2**
5. Caron, M., Touvron, H., Misra, I., Jégou, H., Mairal, J., Bojanowski, P., Joulin, A.: Emerging properties in self-supervised vision transformers. In: *Proceedings of the IEEE/CVF International Conference on Computer Vision*. pp. 9650–9660 (2021) **3**
6. Chen, D.J., Hsieh, H.Y., Liu, T.L.: Adaptive image transformer for one-shot object detection. In: *Proceedings of the IEEE/CVF Conference on Computer Vision and Pattern Recognition*. pp. 12247–12256 (2021) **11**
7. Chen, X., Fang, H., Lin, T.Y., Vedantam, R., Gupta, S., Dollár, P., Zitnick, C.L.: Microsoft coco captions: Data collection and evaluation server. *arXiv preprint arXiv:1504.00325* (2015) **13**
8. Dorogovtsev, S.N., Mendes, J.F.F.: Language as an evolving word web. *Proceedings of the Royal Society of London. Series B: Biological Sciences* **268**(1485), 2603–2606 (2001) **13**
9. Everingham, M., Van Gool, L., Williams, C.K., Winn, J., Zisserman, A.: The pascal visual object classes (voc) challenge. *International journal of computer vision* **88**, 303–338 (2010) **2, 9**
10. Fan, Q., Zhuo, W., Tang, C.K., Tai, Y.W.: Few-shot object detection with attention-rpn and multi-relation detector. In: *Proceedings of the IEEE/CVF conference on computer vision and pattern recognition*. pp. 4013–4022 (2020) **3, 8, 9**
11. Fan, Z., Ma, Y., Li, Z., Sun, J.: Generalized few-shot object detection without forgetting. In: *Proceedings of the IEEE/CVF Conference on Computer Vision and Pattern Recognition*. pp. 4527–4536 (2021) **3, 8, 9**
12. Fang, Y., Sun, Q., Wang, X., Huang, T., Wang, X., Cao, Y.: Eva-02: A visual representation for neon genesis. *arXiv preprint arXiv:2303.11331* (2023) **13**

13. Gu, X., Lin, T.Y., Kuo, W., Cui, Y.: Open-vocabulary object detection via vision and language knowledge distillation. In: International Conference on Learning Representations (2021) [5](#), [12](#)
14. Guirguis, K., Meier, J., Eskandar, G., Kayser, M., Yang, B., Beyerer, J.: Niff: Alleviating forgetting in generalized few-shot object detection via neural instance feature forging. In: Proceedings of the IEEE/CVF Conference on Computer Vision and Pattern Recognition. pp. 24193–24202 (2023) [2](#), [3](#), [8](#), [9](#), [11](#)
15. Gupta, A., Dollar, P., Girshick, R.: Lvis: A dataset for large vocabulary instance segmentation. In: Proceedings of the IEEE/CVF Conference on Computer Vision and Pattern Recognition. pp. 5356–5364 (2019) [2](#), [9](#)
16. Gupta, A., Narayan, S., Joseph, K., Khan, S., Khan, F.S., Shah, M.: Ow-detr: Open-world detection transformer. In: Proceedings of the IEEE/CVF Conference on Computer Vision and Pattern Recognition. pp. 9235–9244 (2022) [3](#)
17. Han, G., He, Y., Huang, S., Ma, J., Chang, S.F.: Query adaptive few-shot object detection with heterogeneous graph convolutional networks. In: Proceedings of the IEEE/CVF International Conference on Computer Vision. pp. 3263–3272 (2021) [3](#), [8](#), [9](#)
18. Han, G., Huang, S., Ma, J., He, Y., Chang, S.F.: Meta faster r-cnn: Towards accurate few-shot object detection with attentive feature alignment. In: Proceedings of the AAAI Conference on Artificial Intelligence. vol. 36, pp. 780–789 (2022) [3](#), [8](#), [9](#), [10](#), [11](#), [12](#)
19. Han, G., Ma, J., Huang, S., Chen, L., Chang, S.F.: Few-shot object detection with fully cross-transformer. In: Proceedings of the IEEE/CVF Conference on Computer Vision and Pattern Recognition. pp. 5321–5330 (2022) [3](#), [8](#), [9](#), [11](#), [12](#)
20. He, K., Gkioxari, G., Dollár, P., Girshick, R.: Mask r-cnn. In: Proceedings of the IEEE International Conference on Computer Vision. pp. 2961–2969 (2017) [9](#)
21. He, K., Zhang, X., Ren, S., Sun, J.: Deep residual learning for image recognition. In: Proceedings of the IEEE conference on computer vision and pattern recognition. pp. 770–778 (2016) [11](#)
22. Hensel, F., Moor, M., Rieck, B.: A survey of topological machine learning methods. *Frontiers in Artificial Intelligence* **4**, 681108 (2021) [8](#)
23. Hsieh, T.I., Lo, Y.C., Chen, H.T., Liu, T.L.: One-shot object detection with co-attention and co-excitation. *Advances in Neural Information Processing Systems* **32** (2019) [11](#)
24. Jolicoeur, P., Gluck, M.A., Kosslyn, S.M.: Pictures and names: Making the connection. *Cognitive psychology* **16**(2), 243–275 (1984) [13](#)
25. Kang, B., Liu, Z., Wang, X., Yu, F., Feng, J., Darrell, T.: Few-shot object detection via feature reweighting. In: Proceedings of the IEEE/CVF International Conference on Computer Vision. pp. 8420–8429 (2019) [3](#), [8](#)
26. Kaul, P., Xie, W., Zisserman, A.: Label, verify, correct: A simple few shot object detection method. In: Proceedings of the IEEE/CVF Conference on Computer Vision and Pattern Recognition. pp. 14237–14247 (2022) [2](#), [8](#), [9](#), [10](#), [12](#)
27. Kim, D., Angelova, A., Kuo, W.: Region-aware pretraining for open-vocabulary object detection with vision transformers. In: Proceedings of the IEEE/CVF Conference on Computer Vision and Pattern Recognition. pp. 11144–11154 (2023) [12](#)
28. Köhler, M., Eisenbach, M., Gross, H.M.: Few-shot object detection: a comprehensive survey. *IEEE Transactions on Neural Networks and Learning Systems* (2023) [1](#), [3](#)
29. Krizhevsky, A., Sutskever, I., Hinton, G.E.: Imagenet classification with deep convolutional neural networks. *Advances in Neural Information Processing Systems* **25** (2012) [13](#)

30. Landau, B., Gleitman, L.R., Landau, B.: Language and experience: Evidence from the blind child, vol. 8. Harvard University Press (2009) [13](#)
31. Lin, T.Y., Maire, M., Belongie, S., Hays, J., Perona, P., Ramanan, D., Dollár, P., Zitnick, C.L.: Microsoft coco: Common objects in context. In: European Conference on Computer Vision. pp. 740–755. Springer (2014) [2](#), [6](#), [9](#)
32. Liu, Z., Lin, Y., Cao, Y., Hu, H., Wei, Y., Zhang, Z., Lin, S., Guo, B.: Swin transformer: Hierarchical vision transformer using shifted windows. In: Proceedings of the IEEE/CVF International Conference on Computer Vision. pp. 10012–10022 (2021) [11](#)
33. Ma, C., Jiang, Y., Wen, X., Yuan, Z., Qi, X.: Codet: Co-occurrence guided region-word alignment for open-vocabulary object detection. *Advances in Neural Information Processing Systems* **36** (2024) [12](#), [13](#)
34. Ma, J., Niu, Y., Xu, J., Huang, S., Han, G., Chang, S.F.: Digeo: Discriminative geometry-aware learning for generalized few-shot object detection. In: Proceedings of the IEEE/CVF Conference on Computer Vision and Pattern Recognition. pp. 3208–3218 (2023) [2](#), [7](#), [8](#), [9](#), [10](#), [11](#)
35. maintainers, T., contributors: Torchvision: Pytorch’s computer vision library. <https://github.com/pytorch/vision> (2016) [6](#)
36. Melas-Kyriazi, L., Rupprecht, C., Laina, I., Vedaldi, A.: Deep spectral methods: A surprisingly strong baseline for unsupervised semantic segmentation and localization. In: Proceedings of the IEEE/CVF Conference on Computer Vision and Pattern Recognition. pp. 8364–8375 (2022) [1](#), [3](#)
37. Michaelis, C., Ustyuzhaninov, I., Bethge, M., Ecker, A.S.: One-shot instance segmentation. arXiv preprint arXiv:1811.11507 (2018) [9](#), [11](#)
38. Minderer, M., Gritsenko, A., Stone, A., Neumann, M., Weissenborn, D., Dosovitskiy, A., Mahendran, A., Arnab, A., Dehghani, M., Shen, Z., et al.: Simple open-vocabulary object detection. In: European Conference on Computer Vision. pp. 728–755. Springer (2022) [11](#), [12](#)
39. Oquab, M., Darcet, T., Moutakanni, T., Vo, H., Szafraniec, M., Khalidov, V., Fernandez, P., Haziza, D., Massa, F., El-Nouby, A., et al.: DINOv2: Learning robust visual features without supervision. arXiv preprint arXiv:2304.07193 (2023) [3](#), [9](#)
40. Ren, T., Liu, S., Li, F., Zhang, H., Zeng, A., Yang, J., Liao, X., Jia, D., Li, H., Cao, H., Wang, J., Zeng, Z., Qi, X., Yuan, Y., Yang, J., Zhang, L.: detrex: Benchmarking detection transformers (2023) [6](#)
41. Salehi, M., Gavves, E., Snoek, C.G., Asano, Y.M.: Time does tell: Self-supervised time-tuning of dense image representations. In: Proceedings of the IEEE/CVF International Conference on Computer Vision. pp. 16536–16547 (2023) [3](#)
42. Schittenkopf, C., Deco, G., Brauer, W.: Two strategies to avoid overfitting in feedforward networks. *Neural Networks* **10**(3), 505–516 (1997). [https://doi.org/https://doi.org/10.1016/S0893-6080\(96\)00086-X](https://doi.org/https://doi.org/10.1016/S0893-6080(96)00086-X), <https://www.sciencedirect.com/science/article/pii/S089360809600086X> [7](#)
43. Siméoni, O., Sekkat, C., Puy, G., Vobecký, A., Zablocki, É., Pérez, P.: Unsupervised object localization: Observing the background to discover objects. In: Proceedings of the IEEE/CVF Conference on Computer Vision and Pattern Recognition. pp. 3176–3186 (2023) [1](#), [3](#)
44. Sudre, C.H., Li, W., Vercauteren, T., Ourselin, S., Jorge Cardoso, M.: Generalised dice overlap as a deep learning loss function for highly unbalanced segmentations. In: Deep Learning in Medical Image Analysis and Multimodal Learning for Clinical Decision Support: Third International Workshop. pp. 240–248. Springer (2017) [6](#)

45. Sun, B., Li, B., Cai, S., Yuan, Y., Zhang, C.: Fscf: Few-shot object detection via contrastive proposal encoding. In: Proceedings of the IEEE/CVF Conference on Computer Vision and Pattern Recognition. pp. 7352–7362 (2021) [3](#), [8](#)
46. Wang, X., Huang, T.E., Darrell, T., Gonzalez, J.E., Yu, F.: Frustratingly simple few-shot object detection. In: Proceedings of the 37th International Conference on Machine Learning. ICML’20, JMLR.org (2020) [2](#), [3](#), [8](#), [9](#), [11](#)
47. Wang, Y., Shen, X., Hu, S.X., Yuan, Y., Crowley, J.L., Vaufreydaz, D.: Self-supervised transformers for unsupervised object discovery using normalized cut. In: Proceedings of the IEEE/CVF Conference on Computer Vision and Pattern Recognition. pp. 14543–14553 (2022) [3](#)
48. Wu, J., Li, X., Yuan, S.X.H., Ding, H., Yang, Y., Li, X., Zhang, J., Tong, Y., Jiang, X., Ghanem, B., et al.: Towards open vocabulary learning: A survey. arXiv preprint arXiv:2306.15880 (2023) [12](#)
49. Wu, X., Zhu, F., Zhao, R., Li, H.: Cora: Adapting clip for open-vocabulary detection with region prompting and anchor pre-matching. In: Proceedings of the IEEE/CVF Conference on Computer Vision and Pattern Recognition. pp. 7031–7040 (2023) [12](#)
50. Xiao, Y., Lepetit, V., Marlet, R.: Few-shot object detection and viewpoint estimation for objects in the wild. IEEE Transactions on Pattern Analysis and Machine Intelligence **45**(3), 3090–3106 (2022) [3](#), [8](#)
51. Yan, X., Chen, Z., Xu, A., Wang, X., Liang, X., Lin, L.: Meta r-cnn: Towards general solver for instance-level low-shot learning. In: Proceedings of the IEEE/CVF International Conference on Computer Vision. pp. 9577–9586 (2019) [3](#), [5](#), [7](#), [8](#), [9](#), [13](#)
52. Yang, H., Cai, S., Sheng, H., Deng, B., Huang, J., Hua, X.S., Tang, Y., Zhang, Y.: Balanced and hierarchical relation learning for one-shot object detection. In: Proceedings of the IEEE/CVF Conference on Computer Vision and Pattern Recognition. pp. 7591–7600 (2022) [2](#), [3](#), [9](#), [11](#)
53. Zang, Y., Li, W., Zhou, K., Huang, C., Loy, C.C.: Open-vocabulary detr with conditional matching. In: European Conference on Computer Vision. pp. 106–122. Springer (2022) [12](#)
54. Zhang, X., Boularias, A.: Optical flow boosts unsupervised localization and segmentation. In: 2023 IEEE/RSJ International Conference on Intelligent Robots and Systems (IROS). pp. 7635–7642. IEEE (2023) [3](#)
55. Zhao, Y., Guo, X., Lu, Y.: Semantic-aligned fusion transformer for one-shot object detection. In: Proceedings of the IEEE/CVF Conference on Computer Vision and Pattern Recognition. pp. 7601–7611 (2022) [1](#), [3](#), [11](#)
56. Zhong, Y., Yang, J., Zhang, P., Li, C., Codella, N., Li, L.H., Zhou, L., Dai, X., Yuan, L., Li, Y., et al.: Regionclip: Region-based language-image pretraining. In: Proceedings of the IEEE/CVF Conference on Computer Vision and Pattern Recognition. pp. 16793–16803 (2022) [9](#), [12](#)
57. Zhou, B., Zhao, H., Puig, X., Fidler, S., Barriuso, A., Torrallba, A.: Scene parsing through ade20k dataset. In: Proceedings of the IEEE conference on computer vision and pattern recognition. pp. 633–641 (2017) [13](#), [14](#)
58. Zhou, X., Girdhar, R., Joulin, A., Krähenbühl, P., Misra, I.: Detecting twenty-thousand classes using image-level supervision. In: European Conference on Computer Vision. pp. 350–368. Springer (2022) [12](#)
59. Ziegler, A., Asano, Y.M.: Self-supervised learning of object parts for semantic segmentation. In: Proceedings of the IEEE/CVF Conference on Computer Vision and Pattern Recognition. pp. 14502–14511 (2022) [3](#)